JACS
JOURNAL OF THE AMERICAN CHEMICAL SOCIETY

Article

pubs.acs.org/JACS

Electron Spin Density Distribution in the Special Pair Triplet of *Rhodobacter sphaeroides* R26 Revealed by Magnetic Field Dependence of the Solid-State Photo-CIDNP Effect

Smitha Surendran Thamarath,[†] Bela E. Bode,[†,‡] Shipra Prakash,[†] Karthick Babu Sai Sankar Gupta,[†] A. Alia,[†] Gunnar Jeschke,*[,§] and Jörg Matysik*[,†]

[†]Leiden Institute of Chemistry, Leiden University, 2300 RA Leiden, The Netherlands
[‡]EaStCHEM and Biomedical Sciences Research Complex, University of St Andrews, St Andrews, KY16 9ST, Scotland
[§]Institut für Physikalische Chemie, Eidgenössische Technische Hochschule, Zürich, Switzerland

Ⓢ *Supporting Information*

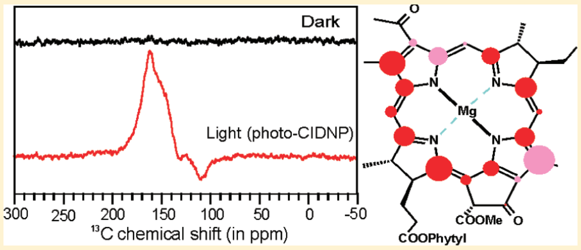

ABSTRACT: Photo-CIDNP (photochemically induced dynamic nuclear polarization) can be observed in frozen and quinone-blocked photosynthetic reaction centers (RCs) as modification of magic-angle spinning (MAS) NMR signal intensity under illumination. Studying the carotenoidless mutant strain R26 of *Rhodobacter sphaeroides*, we demonstrate by experiment and theory that contributions to the nuclear spin polarization from the three-spin mixing and differential decay mechanism can be separated from polarization generated by the radical pair mechanism, which is partially maintained due to differential relaxation (DR) in the singlet and triplet branch. At a magnetic field of 1.4 T, the latter contribution leads to dramatic signal enhancement of about 80 000 and dominates over the two other mechanisms. The DR mechanism encodes information on the spin density distribution in the donor triplet state. Relative peak intensities in the photo-CIDNP spectra provide a critical test for triplet spin densities computed for different model chemistries and conformations. The unpaired electrons are distributed almost evenly over the two moieties of the special pair of bacteriochlorophylls, with only slight excess in the L branch.

■ INTRODUCTION

Optical nuclear polarization (ONP) associated with triplet states in molecular crystals was discovered in 1967[1] and the underlying mechanism was fully understood by 1977.[2] As the effects depend on a level anticrossing induced by matching of the zero-field splitting with the electron Zeeman frequency, ONP theory could not explain the solid-state photo-CIDNP effect at high fields, discovered by M. Zysmilich and A. McDermott in 1994 on photosynthetic reaction centers,[3] whose triplet states feature rather small zero-field splitting. The solid-state photo-CIDNP effect provides a method to overcome the intrinsically low sensitivity of NMR by generation of non-Boltzmann populations of nuclear spin states by photochemical reactions in solids (for review, see refs 4, 5). This photochemically induced dynamic nuclear polarization (photo-CIDNP) can be detected by magic-angle spinning (MAS) NMR as strong modification of signal intensities. Enhancement factors of above 10 000 have been reported for ^{13}C MAS NMR at a magnetic field of 4.7 T (i.e., 200 MHz ^{1}H frequency and 50 MHz ^{13}C frequency) in photosynthetic reaction centers (RCs) of the purple bacteria *Rhodobacter sphaeroides* wildtype (WT)[6] and the carotenoidless mutant R26.[7] Such strong signal enhancement allows, for example, for highly selective observation of the photosynthetic cofactors at nanomolar concentrations in entire cells.[7,8] Because of the long ^{13}C relaxation time in solids, the nuclear polarization of subsequent photocycles can be accumulated in continuous illumination experiments making photo-CIDNP MAS NMR a sensitive analytical tool for systems in which the effect is observed.[9−13] The effect has been observed in all natural photosynthetic RCs studied so far. It appears to be an intrinsic property of natural photosynthesis and has been proposed to be related to efficient electron transfer.[14] For a long time, experiments on systems other than natural photosynthetic RCs failed. Recently, however, the effect was observed in a blue-light photoreceptor, the phototropin mutant LOV1-C57S at 2.4 T demonstrating that the effect is not limited to natural photosynthesis.[15]

The cyclic spin-chemical processes producing such high nuclear polarizations are now understood for a spin-correlated radical pair interacting with a single nuclear spin in the high-field limit in quinone-removed RCs of *R. sphaeroides*.[4,16] Under illumination, the well-studied RCs of *R. sphaeroides*[17,18] form radical pairs with the primary electron donor P, the so-called "special pair" of two bacteriochlorophylls (BChl) as radical cation and the primary electron acceptor Φ, a bacteriopheophytin (BPhe), as radical anion (Scheme 1). The initial electron spin zero-quantum coherence, which is created upon birth of the radical pair in the S state in the S−T$_0$ manifold of states, is transferred by two coherent solid-state mechanisms, the three-

Received: December 30, 2011
Published: March 7, 2012

Scheme 1. Photocycle in Quinone-Blocked RCs of *R. sphaeroides* WT and R26[a]

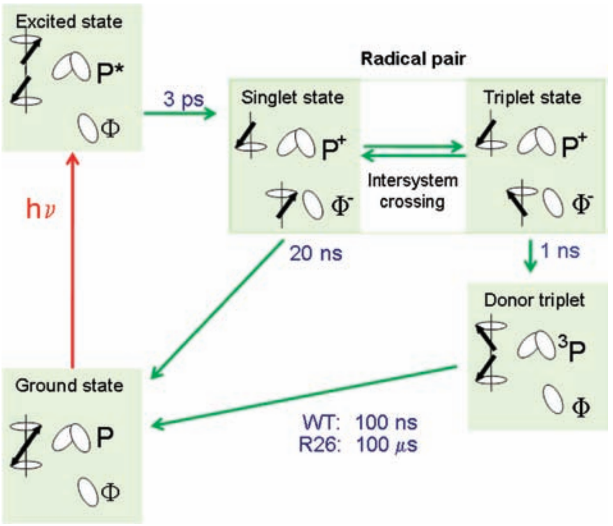

[a]Upon illumination and fast electron transfer from an excited singlet state, a radical pair is formed in a pure singlet state having high electron spin order. The radical pair is formed by a radical cation at the two donor BChls (Special pair, P) and a radical anion on the BPhe acceptor cofactor (Φ) of the active branch. The chemical fate of the radical pair depends on its electronic spin state: while the singlet state is allowed to recombine, for the triplet state a direct recombination is spin-forbidden and a donor triplet (^{3}P) is formed by inter-system crossing. The lifetime of ^{3}P depends on the relaxation channels provided by the environment. Therefore, it is short in WT RCs having a nearby carotenoid and significantly longer in the carotenoidless mutant R26.

spin mixing (TSM).[19,20] and the differential decay (DD),[21] into *net* nuclear polarization. In the electron−electron-nuclear TSM mechanism, the symmetry of the coherent spin evolution in the correlated radical pair is broken by state mixing due to anisotropic electron−electron dipolar coupling and pseudosecular hyperfine coupling (hfc). State mixing is maximized at the double matching condition $2|\Delta\Omega| = 2|\omega_I| = |A|$, that is, the difference of the electron Zeeman frequencies $\Delta\Omega$, the nuclear Zeeman frequency ω_I, and the secular part of the hyperfine interaction A must match. In the DD mechanism, this symmetry is broken by different lifetimes of the S and of the T_0 states and by pseudosecular hyperfine coupling. In this case, only a single matching of interactions $2|\omega_I| = |A|$ is required and the difference of singlet and triplet radical pair lifetimes must be of the order of the inverse hfc. During the radical pair evolution, the occurrence of these two competing mechanisms in RCs of *R. sphaeroides* WT leads to a set of entirely emissive (negative) signals, whose relative intensity encodes information on spin density distribution in the radical pair state.[6] Since $\Delta\Omega$ and ω_I depend on the magnetic field, while A does not, both the TSM and DD mechanism create maximum absolute nuclear polarization at a matching field.

In RCs having a long donor triplet lifetime as in the carotenoidless mutant R26 of *R. sphaeroides*, contributions from a third mechanism have been observed.[7] In this situation, polarization generated by the radical pair mechanism (RPM),[22,23] which has the same amplitude and opposite sign in the singlet and triplet branch and thus usually cancels in cyclic reactions, is partially maintained[24,25] due to different longitudinal nuclear relaxation in the two branches (for review, see ref 26). In the solid state, this has been termed the differential relaxation (DR) mechanism to emphasize that RPM polarization is modified according to the different relaxation rates for different nuclei.[4] This mechanism explains the differences between photo-CIDNP spectra of RCs of *R. sphaeroides* WT and R26.[7] The DR mechanism relies on enhanced nuclear relaxation in the triplet branch, which is in turn caused by fluctuations of the anisotropic hyperfine couplings of these nuclei to the donor triplet (^{3}P) state. Therefore, relative line intensity in this case also encodes information on spin density distribution in the ^{3}P state.[7] Such information is of interest to understand photoprotection of the RCs by fast triplet quenching.[17] Furthermore, studies of the triplet state of bacterial RCs have provided insight into the strongly asymmetric distribution of electron transfer between the nearly symmetric M and L branches of bacterial RCs.[27,28]

Unfortunately, all three mechanisms are operative simultaneously. Furthermore, even for the DR mechanism, relative line intensities depend on spin density distribution in both the radical pair state (through the RPM) and the donor triplet state (through paramagnetically induced relaxation). In the present work, we show that the contributions can be disentangled. For this, we rely on separate characterization of the RPM polarization by time-resolved ^{13}C photo-CIDNP MAS NMR[29] and on different field dependences of the three mechanisms. Previous experimental studies on both RC types WT and R26 clearly demonstrated a strong increase of the photo-CIDNP enhancement with lower fields between 17.4 and 4.7 T.[6,7] From experiment, it is not known whether the enhancement further increases and at which field a maximum occurs. The discovery of the effect in a nonphotosynthetic system occurred at an even lower field of 2.4 T.[15] Simulation of the coherent TSM and DD mechanism for photosynthetic RCs suggests a maximum polarization at ≈2 T,[30] which has not been experimentally evidenced to date. Although we lack information on the relaxation dispersion of the electron spin in the donor triplet ^{3}P, relaxation theory suggests that for the expected electron spin relaxation times in the microsecond range paramagnetic relaxation enhancement increases down to fields well below 2 T. Accordingly, DR polarization should dominate at sufficiently low fields. Here, we provide an experimental "trial drill" toward lower fields as far as commercial NMR hardware allows. At these fields of 1.4 and 2.4 T, coherent evolution is still strictly within the S−T_0 manifolds, and a newly proposed TSM mechanism based on S−T_- mixing[31] can be safely neglected.

■ RESULTS

Figures 1 and 2 demonstrate the amplitude of the solid-state photo-CIDNP effect in the magnetic field range from 2.4 to 17.6 T in WT and R26, respectively. In this regime, ^{13}C MAS NMR spectra can be detected straightforwardly under ^{1}H decoupling. While dark experiments (spectra shown in black) show an increase in signal intensity and resolution toward higher fields, the light-induced signals (spectra shown in red) show the opposite trend. The lower the field, the stronger the intensity of the light induced signals. The optimum for the spectral resolution is reached at about 4.7 T (200 MHz ^{1}H frequency), since at 2.4 T, the spectral dispersion becomes too poor, while at higher field, artificial line-broadening is required to compensate for low signal-to-noise ratio. In this field range, these trends hold for both RCs, WT (Figure 1) and R26

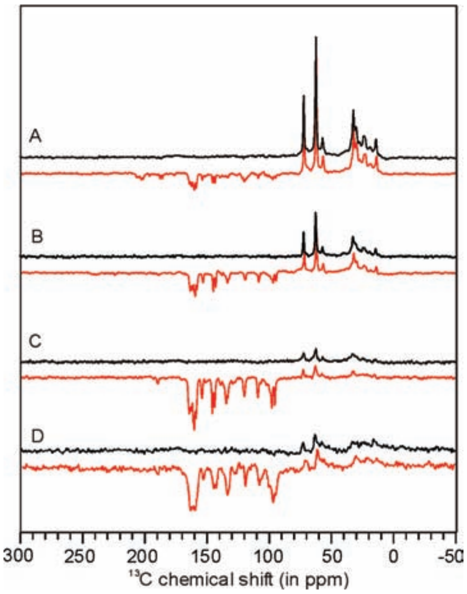

Figure 1. ^{13}C MAS NMR spectra of quinone depleted RCs of *R. sphaeroides* WT in the dark (black) and under illumination (red) at 17.6 (A), 9.4 (B), 4.7 (C), and 2.4 T (D). The spectra were obtained at 235 K under a MAS frequency of 8 kHz under ^{1}H decoupling.

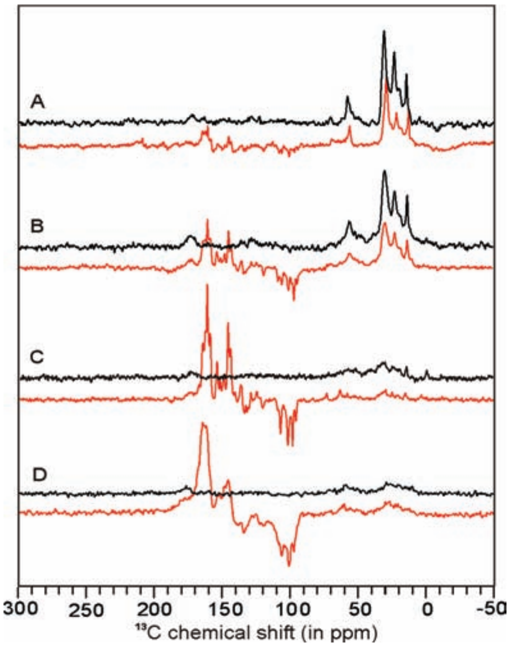

Figure 2. ^{13}C MAS NMR spectra of quinone depleted RCs of *R. sphaeroides* R26 in the dark (black) and under illumination (red) at 17.6 (A), 9.4 (B), 4.7 (C), and 2.4 T (D). The spectra were obtained at 235 K under a MAS frequency of 8 kHz under ^{1}H decoupling.

(Figure 2). Hence, the question arises whether the enhancement further increases at even lower fields.

Within the entire field regime, the intensity patterns are different between spectra of WT and R26 RCs. While the first are entirely emissive spectra, in the latter both emissive and absorptive lines occur. Previous analysis has shown that a set of entirely emissive signals originates from both donor and acceptor of the primary radical pair of WT RCs (Figure 1).[6,16] This nonequilibrium polarization has been interpreted in terms of competing TSM and DD mechanisms. The all-emissive spectrum is caused by a predominance of the TSM over the DD mechanism, for which the sign of the signal depends on the signs of the secular hyperfine coupling and of the *g* tensor difference.[4] In R26 RCs, the DR mechanism leads to admixture of polarization from the RPM for those donor nuclei that exhibit strongly anisotropic hyperfine couplings in the ^{3}P state. For positive isotropic hyperfine couplings in the radical pair state, this DR polarization is absorptive, while it is emissive for negative isotropic hyperfine couplings in the radical pair state. This sign rule may be violated if the anisotropic contribution strongly dominates the isotropic contribution to the hyperfine coupling in the radical pair state. It is expected that the field dependence of the TSM, DD, and DR mechanisms is different implying that also the spectral pattern changes with the field. In Figure 2, however, the ratio of negative to positive signals appears to depend only weakly on field.

At fields below 2.4 T, our hardware does not allow for ^{1}H decoupling. To compare the effect of decoupling on the spectra, we measured ^{1}H−coupled and decoupled spectra for both samples (Figures S1 and S2) at this field. The comparison shows that in particular the signals around 100 ppm originating from methine bridge carbons, which are directly bound to a proton, are broadened beyond detection in the ^{1}H-coupled spectra while the other signals just broaden substantially.

Experiments at 2.4 and 1.4 T (100 and 60 MHz ^{1}H frequency, respectively) for RCs of WT and R26 are shown in Figures 3 and 4. In Figure 3 the effect considerably weakens toward lower fields. Hence, our data provide empirical evidence that the coherent high-field solid-state photo-CIDNP effect for bacterial RCs shows a maximum around 2.4 T. In Figure 4, on the other hand, the light-induced positive feature strongly increases toward lower field. The ratio between positive and negative signals is changed strongly in favor of the first. Thus, while the TSM and DD mechanisms become less efficient at 1.4 T, the DR mechanism becomes more potent. Experiments at even lower fields would require a different type of hardware.

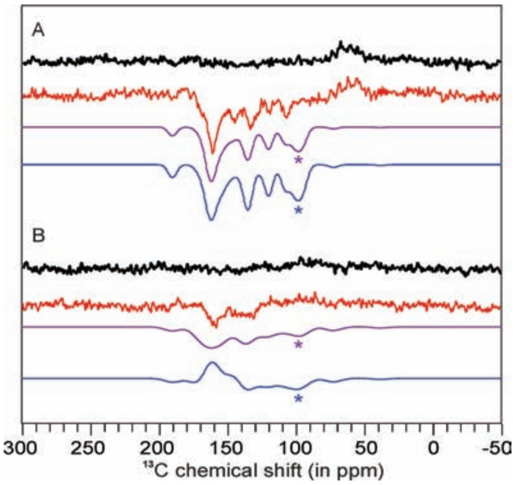

Figure 3. ^{13}C MAS NMR spectra of quinone depleted RCs of *R. sphaeroides* WT in the dark (black) and under illumination (red) as well as numerical simulations of the photo-CIDNP effect with T_{1T} = 100 ns (lilac) and T_{1T} = 56 ns (blue) at 2.4 (A) and 1.4 T (B). The experimental data were obtained at 235 K under an MAS frequency of 8 kHz without ^{1}H decoupling. The asterisks mark methine carbon signals that are lost without decoupling.

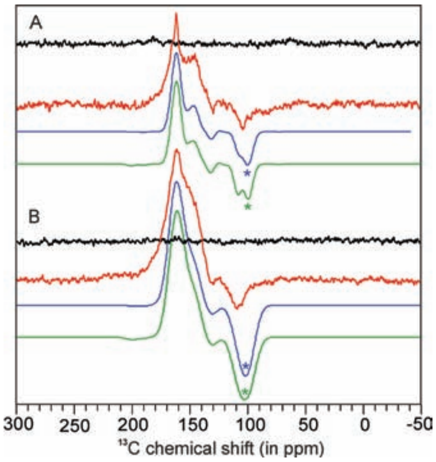

Figure 4. ^{13}C MAS NMR spectra of quinone depleted RCs of *R. sphaeroides* R26 in the dark (black) and under illumination (red) as well as numerical simulations of the photo-CIDNP effect with T_{1T} = 56 ns and triplet spin density from DFT computations with the BLYP functional (blue) and the BP86 functional (green) at 2.4 (A) and 1.4 T (B). The experimental data were obtained at 235 K under an MAS frequency of 8 kHz without ^{1}H decoupling. The asterisks mark methine carbon signals that are lost without decoupling.

In particular, a field cycling system would be suitable to avoid further loss of resolution.

All spectra are presented with similar signal-to-noise ratio within a figure. In previous work, using the response of the methyl groups as an internal standard for estimating the enhancement factor of the solid-state photo-CIDNP effect, this factor was found to be about 10 000 at a magnetic field of 4.7 T.[6,7] The methyl signal at 30 ppm corresponds to the 3300 methyl groups in the RC protein. The experiments at 2.4 T for RCs of WT and R26 show larger enhancement compared to 4.7 T. Using the same standard for the spectra obtained at 2.4 T, enhancement factors have been determined to be 20 000 for WT RCs and 40 000 for R26 RCs.

Because proton decoupling is not feasible with our spectrometer at a magnetic field below 2.4 T, the enhancement factor cannot be calculated as above. It is, however, possible to estimate the enhancement factor in R26 RCs by comparing the spectra without proton decoupling at 2.4 and 1.4 T on the same sample in the same measurement time (Figure 4, red spectra) and assuming that the factor 40 000 is also valid for the spectrum obtained without ^{1}H decoupling. To that end, the absorptive and emissive signals are integrated in the spectra of R26 RCs at the magnetic fields of 2.4 and 1.4 T. The ratio of emissive to absorptive signals appears to be twice at the magnetic field of 1.4 T than that at 2.4 T. If we assume that the DD/TSM contribution remains the same on decreasing the field, the enhancement factor for R26 RCs at 1.4 T can be estimated as 80 000. This is a lower limit, since our simulations (vide infra) indicate that the DD/TSM contribution decreases between 2.4 and 1.4 T.

These results indicate that at the lowest fields indeed contributions from the DR mechanism dominate, which gives rise to the opportunity of characterizing the spin density distribution in ^{3}P state of the special pair. To do so, we need an estimate of the nuclear polarization that is generated by the RPM in the singlet and triplet branch with opposite signs. In principle, such an estimate can be obtained from simulations. For this, experimentally unknown ^{13}C hfc values in the radical pair state are required, which can be estimated by density functional theory (DFT) computations.[6,7] This approach does, however, introduce uncertainty from deviations between DFT computed and true hfc's.

Here, we follow a different route, where the RPM polarization pattern is taken from time-resolved photo-CIDNP MAS NMR experiments that observe the spectrum immediately after a single photocycle has been initiated by a laser pulse.[29] At that time, polarization from the singlet branch is selectively detected, as RCs in the triplet branch are still in a paramagnetic state which shifts and broadens the NMR signals beyond detection. We have fitted the spectrum of *R. sphaeroides* R26 RCs obtained immediately after the nanosecond flash at 4.7 T[29] by scaling nuclear polarization values from a DFT-based computation (Figure S3).

Such fits provide a table of scaling factors for the RPM polarization computed in our simulations. We apply these fitted scaling factors to all further simulations, although strictly they apply only at 4.7 T. The scaling factors typically correspond to an increase or decrease of RPM polarization by 20−30%, although a few signals had to be suppressed by scaling them down by a factor of 10. By comparing simulations with and without such scaling to the experimental spectra, we checked that RPM polarization scaled by these experimentally derived factors provides a better approximation at the other fields than the RPM polarization simulated directly from DFT-computed hfcs.

To simulate polarizations from the DR mechanism, we further need the nuclear longitudinal relaxation times $T_{1n,k}$ in the ^{3}P state. In a first exploration of the DR mechanism,[32] McDermott et al. pointed out that Redfield relaxation theory is probably not applicable to the triplet state of the special pair and used a uniform *ad hoc* relaxation time of 300 s^{-1} to fit ^{15}N photo-CIDNP MAS NMR data. Here, we use the Redfield theory expression

$$T_{1n,k} = 45\omega_I^{\,2}T_{1T}/(4\Delta A_k^{\,2}) \qquad (1)$$

as an approximation, where $\Delta A_k = 3(A_{z,k} - a_{\mathrm{iso},k})/2$ is the hyperfine anisotropy of nucleus k, ω_I is the nuclear Zeeman frequency, which scales linearly with magnetic field, and T_{1T} is the longitudinal electron spin relaxation time in the ^{3}P state. Equation 1 can be obtained from an expression given for paramagnetic relaxation in solids by Abragam[33] by replacing the distance-dependent dipole−dipole coupling between electron and nuclear spin by the anisotropic hfc, which is largely due to spin density in p_z orbitals, and assuming $|\omega_I T_{1T}| \gg 1$, which applies for all magnetic fields used in this work.

From measurements of T_{1T} in *R. sphaeroides* R26 RCs along the *Y* axis of the zero-field splitting tensor at a temperature of 233 K and a field of approximately 0.35 T,[34] we expect that T_{1T} is in the microsecond range. Our DFT computations show that the ΔA_k for the nuclei with the largest spin density are of the order of $2\pi\cdot 10$ MHz (Table S1). Hence, the Redfield regime condition $\Delta A_k T_{1T}/3 \ll 1$ is indeed violated for T_{1T} larger than about 20 ns. We proceed with the Redfield regime approximation nevertheless and discuss uncertainties below. In future work, we shall numerically explore deviations from the Redfield approximation. Preliminary computations for electron spin 1/2 indicate that the approximation remains valid throughout the range of T_{1T} and ΔA_k encountered in this work.

Estimates for the ΔA_k in eq 1 were obtained by two DFT computations for the triplet state of the special pair. The first computation, used already in Prakash et al.[7] was based on nonoptimized heavy atom coordinates of the X-ray crystal structure of R26 RCs in the charge neutral state (PDB 1AIJ).[35] Protons were attached with standard bond lengths and geometries and a spin-unrestricted computation with the BLYP functional was performed.[36,37] This leads to a spin density that is almost symmetrically distributed over the two moieties of the special pair, with only a slight excess in the L moiety (Figure 5).

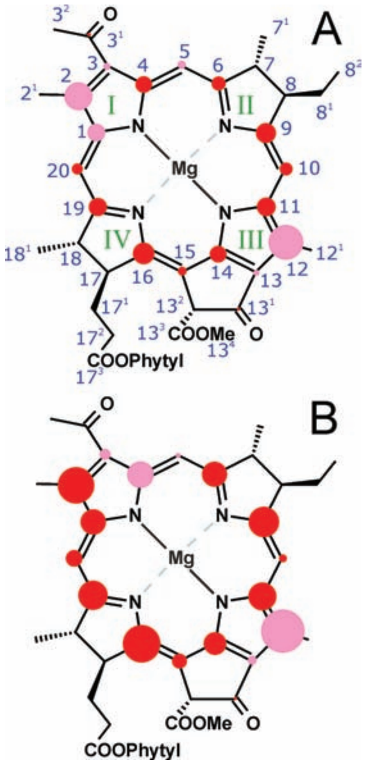

Figure 5. Spin density distribution in the special pair triplet state visualized via relative anisotropic ^{13}C hfc's computed by DFT with the BLYP functional in the M (A) and L (B) moiety. Atom numbering is shown in blue. A circle diameter of one carbon−carbon bond length corresponds to $\Delta A_k = 2\pi\cdot 15$ MHz. Red circles correspond to hyperfine anisotropies that can be experimentally tested, while pink circles correspond to untested ones.

In the second DFT computation, the WT special pair structure was optimized in TURBOMOLE[38] first for the radical cation state and then for the triplet state and hfc's were obtained by a spin-unrestricted computation with the BP86 functional.[36,39] Surprisingly, this led to a completely asymmetrical spin density distribution with both unpaired electrons being localized almost exclusively on the L moiety (Figure S4).

We have tested whether the experimental data can reject one of these two predictions. For that we have simulated the spectra by an approach similar to the one used in Prakash et al.[7] Nuclear polarization after a single photocycle for R26 RCs for the singlet branch ($p_{\mathrm{S},k}$) and triplet branch ($p_{\mathrm{T},k}$) due to RPM, and the TSM and DD mechanisms was computed by density operator formalism. Polarization p_k after return of molecules from both branches to the ground state was taken as an approximation for the steady-state polarization observed in our experiments. This is computed by

$$p_k = p_{s,k} + [1 - \exp(-\tau_{\mathrm{T}}/T_{1\mathrm{n},k})]p_{\mathrm{T},k} \qquad (2)$$

where τ_{T} is the triplet lifetime (100 μs for R26 and 0.1 μs for WT RCs) and the $T_{1\mathrm{n},k}$ values are calculated by eq 1. For a given spectrum, $T_{1\mathrm{T}}$ in eq 1 is the only fit parameter. Finally, the p_k values were multiplied by the experimental RPM scaling factors that we had obtained by fitting time-resolved photo-CIDNP MAS NMR spectra at 4.7 T (vide supra).

The most critical test can thus be performed with the spectrum at 4.7 T (Figure 6). We obtain the best fit for both sets of ΔA_k with $T_{1\mathrm{T}}$ = 56 ns. In general, the agreement between experiment and simulation is better for the BLYP computation without geometry optimization of the R26 structure (blue) than for the BP86 computation after geometry optimization of the WT structure (green). In particular, in the chemical shift range between 141 and 156 ppm (overbars), the number of signals differs between the two simulations and only the BLYP simulation agrees with experiment.

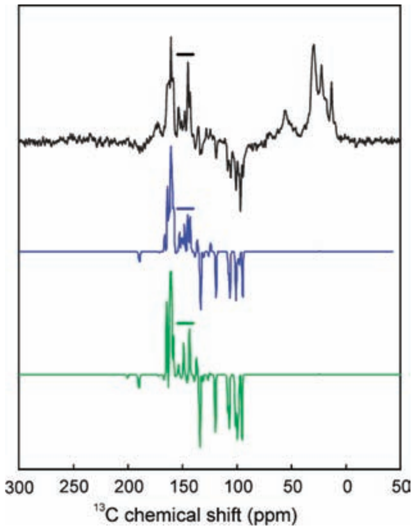

Figure 6. ^{13}C MAS NMR spectrum of quinone depleted RCs of *R. sphaeroides* R26 under illumination at 4.7 T (black) as well as numerical simulations of the photo-CIDNP effect with $T_{1\mathrm{T}}$ = 56 ns and triplet spin density from DFT computations with the BLYP functional (blue) and the BP86 functional (green). The bars denote a spectral range where the number of signals differs in the two simulations.

The same observation can be made in the spectrum at 9.4 T, which is also best fitted with $T_{1\mathrm{T}}$ = 56 ns. From the detail plot shown in Figure 7, it becomes clear that signals from both moieties are experimentally observed with similar intensity, as is predicted by the BLYP computation without geometry optimization of the R26 structure, but not by the BP86 simulation with geometry optimization of the WT structure (see Figure S5 for simulation of the complete spectrum). Note also that sensitivity to the differences in triplet spin density is largely lost in the spectra obtained without ^{1}H decoupling at 2.4 and 1.4 T.

We now turn to a possible field dependence of $T_{1\mathrm{T}}$. Simulation of the ^{13}C photo-CIDNP MAS NMR spectrum of R26 RCs at 17.6 T with the same value $T_{1\mathrm{T}}$ = 56 ns that led to the best fits at 4.7 and 9.4 T results in an overestimate of the

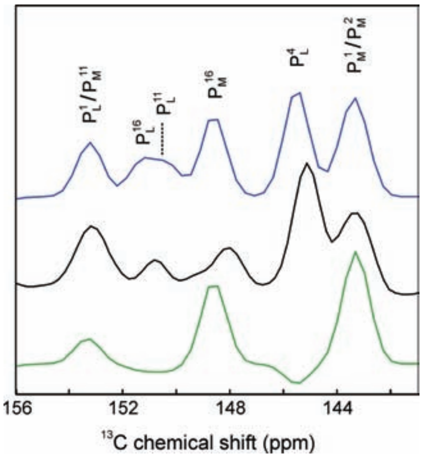

Figure 7. Detail of the ^{13}C MAS NMR spectrum of quinone depleted RCs of *R. sphaeroides* R26 under illumination at 9.4 T (black) as well as numerical simulations of the photo-CIDNP effect with T_{1T} = 56 ns and triplet spin density from DFT computations with the BLYP functional (blue) and the BP86 functional (green).

emissive signal intensity compared to the enhanced absorptive intensity (compare black and blue spectra in Figure 8). At this field, the best overall fit quality is obtained with T_{1T} between 11 and 22 ns (red and lilac line). At the lowest field where we have obtained a decoupled spectrum (2.4 T), relative peak intensities depend rather weakly on T_{1T} (Figure 9). This is because already at T_{1T} = 222 ns (orange spectrum), the prefactor $1 - \exp(-\tau_T/T_{1n,k})$ in eq 2 is close to zero for most nuclei with significant RPM intensity. Fit quality only slightly improves at T_{1T} = 111 ns (not shown) and 56 ns (blue) and degrades again toward shorter T_{1T}.

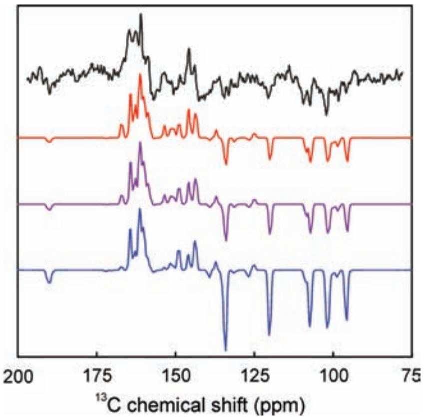

Figure 8. Detail of the ^{13}C MAS NMR spectrum of quinone depleted RCs of *R. sphaeroides* R26 under illumination at 17.6 T (black) as well as numerical simulations of the photo-CIDNP effect triplet spin density from DFT computations with the BLYP functional at T_{1T} = 56 ns. (blue), T_{1T} =22 ns (lilac), and T_{1T} = 11 ns (red).

In contrast, in simulations of the WT spectra with τ_T = 100 ns at 2.4 and 1.4 T, a marked dependence on T_{1T} in that range is detected (Figure 3). Because of the inverse square dependence of the relaxation rate $1/T_{1n,k}$ implied by eq 1, nuclear spin relaxation in the triplet branch can potentially become significant at such fields even for the short-lived triplet state in WT RCs. For WT RCs, we can thus safely exclude that T_{1T} is as short as 56 ns at 1.4 T. In fact, any $T_{1T} \geq 100$ ns provides acceptable fits given the poor signal-to-noise ratio of these spectra, so that we can only derive a lower limit of T_{1T}, although line shapes slightly change at longer T_{1T}.

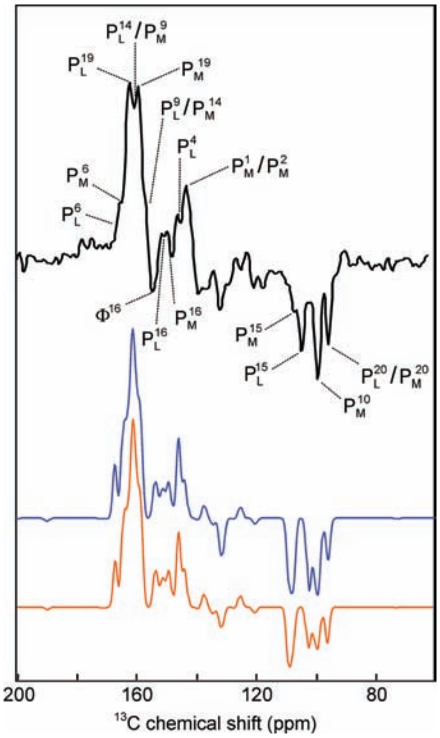

Figure 9. Detail of the ^{13}C MAS NMR spectrum of quinone depleted RCs of *R. sphaeroides* R26 under illumination at 2.4 T (black) as well as numerical simulations of the photo-CIDNP effect triplet spin density from DFT computations with the BLYP functional at T_{1T} = 56 ns (blue) and T_{1T} = 222 ns (orange). To enhance resolution for peak assignment, the experimental spectrum was subjected to a line-narrowing Lorentz-Gauss transformation.

For simulations of the field dependence of polarization due to the DR mechanism, we assume an empirical power law $T_{1T} = 22.2\cdot(17.6\ \mathrm{T}/B_0)^{0.69}$ ns, where B_0 is the magnetic field. The prefactor and exponent were chosen such that the best fitting T_{1T} values are obtained at 17.6 and 4.7 T. This empirical choice fits all R26 spectra (Figure S6) and the WT spectra at 1.4 and 2.4 T (Figure S7) with acceptable quality. The WT spectra at higher fields are insensitive to the choice of T_{1T}. At a field of 0.35 T, the empirical power law predicts $T_{1T} \approx 0.33\ \mu$s, which is by a factor of about 7.5 lower than the value of 2.5 μs measured at 233 K along the *y* axis of the zero-field splitting tensor by Hoff et al.[34] Note that the temperature inside the MAS rotor at 8 kHz spinning frequency may be ~5 K higher than the controlled temperature of the cooling gas, which in our case is 235 K. Since the temperature is close to the glass transition temperature of the sample and the EPR signal of ^{3}P is lost at higher temperatures by faster relaxation,[34] a sample temperature increase by a few degree may well explain the difference between the ^{3}P longitudinal relaxation time predicted at 0.35 T from our data and the one measured at 233 K by Hoff et al. Furthermore, the data by Hoff et al. indicate shorter relaxation times along the other axes of the zero-field splitting tensor, which could not be quantified at the sensitivity achieved in their experiments.

Because of the square dependence of the $T_{1n,k}$ on ω_I and thus B_0 implied by eq 1, the empirical power law for T_{1T} leads to a $B_0^{1.31}$ scaling of the $T_{1n,k}$. According to eq 2, such shortening of the $T_{1n,k}$ with decreasing field in turn leads to $p_k = p_{S,k}$ at sufficiently low field. Under such conditions, the full nuclear polarization due to the RPM would be maintained and the Kaptein sign rules[40] for cage products would apply.

The trend in nuclear polarization predicted from such simulations is in qualitative agreement with experimental observations (Figure 10A and S8A). For WT RCs, maximum emissive polarization is expected around 4.7 T, whereas polarization is very small at 1.4 T. We have also computed polarization at fields of 0.96, 0.48, and 0.24 T. These data points suggest that at even lower fields absorptive polarization due to the DR mechanism should appear. Note, however, that NMR sensitivity at given nuclear polarization scales with the square root of magnetic field. If this scaling is taken into account, maximum sensitivity in the low-field emissive spectra is expected to be about the same as in the absorptive spectra at 2.4 T and certainly worse than at 4.7 T. Comparison of Figures S8A and S9A reveals that the emissive polarization in WT RCs at fields lower than 1.4 T is due to the DR mechanism, since it vanishes at infinite T_{1T}.

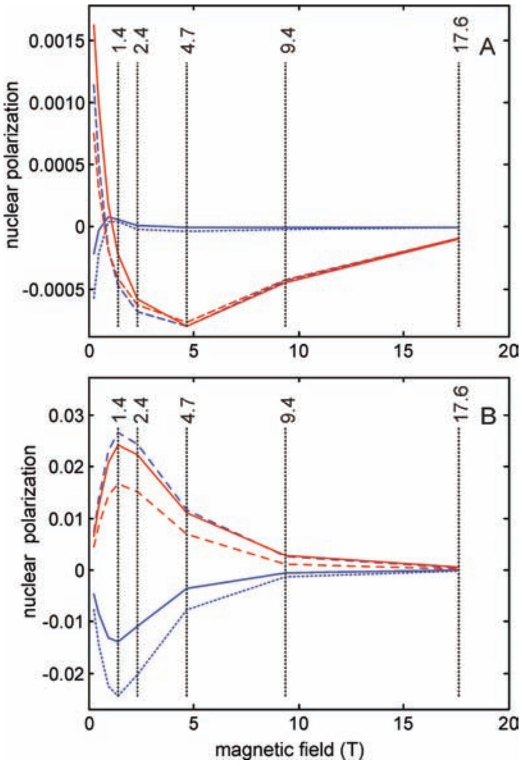

Figure 10. Simulated field dependence of donor nuclear polarization for selected nuclei of WT (A) and R26 (B) RCs of *R. sphaeroides*, assuming $T_{1T} = 22.2(17.6\ \mathrm{T}/B_0)^{0.69}$ ns and triplet hfc's from a DFT computation with the BLYP functional without geometry optimization of the crystal structure. Blue lines correspond to the L moiety, $P_L{}^4$ solid line, $P_L{}^{14}$ dashed, $P_L{}^{15}$ dotted. Red lines correspond do the M moiety. $P_M{}^{10}$ solid, $P_M{}^{16}$ dashed. Black dotted vertical lines denote fields were measurements were performed.

For R26 RCs, maximum nuclear polarization is predicted around 1.4 T, although sensitivity at the same line width may be slightly better at 2.4 T (Figure 10B and S8B). The contribution of acceptor signals (maximum polarization corresponding to the blue dashed line) is comparable to the emissive donor signals at 4.7 T and much smaller than those signals at 2.4 and 1.4 T. For the field dependence of acceptor nuclear polarization due to the TSM and DD mechanisms, see Figure S9B.

Quantitative comparison of the experimental and simulated field dependence of signal intensity is hampered by the fact that the experimental intensities at low fields cannot reliably be normalized. Signal-to-noise ratio for the reference signal in the dark spectrum is poor already at 4.7 T, very poor at 2.4 T, and the signal is not detected in the spectrum without decoupling at 1.4 T. Therefore, we refrain from quantitative comparison.

■ DISCUSSION

1. Triplet Spin Densities. Our conclusions on electronic structure of the special pair triplet depend on the scaling of nuclear longitudinal relaxation times with the $\Delta A_k{}^2$ suggested by the Redfield-regime expression in eq 1. Although not all conditions for the Redfield approximation are strictly fulfilled, the one about scaling with $\Delta A_k{}^2$ is expected to hold as long as $\Delta A_k \ll 2\omega_I$. This condition is certainly fulfilled at 9.4 T, where $2\omega_I/\Delta A_k > 12$ for all nuclei. Hence, the data shown in Figure 7 are unequivocal evidence for an approximately symmetric distribution of spin density over the two moieties of the special pair as opposed to a strongly biased one.

We now turn to the question to what extent the symmetric spin density distribution suggested in Figure 5 on the basis of a DFT computation is actually tested by our experiments. Observation of the DR effect and thus any conclusion on a ΔA_k in the triplet state depends on significant RPM polarization for this nucleus. This in turn requires at least a moderate hyperfine coupling of this nucleus in the radical pair state. This condition is fulfilled for all nuclei whose signals we could assign in Figure 7 or 9. The corresponding circles for the ΔA_k in the triplet state are shown in red color in Figure 5. For the nuclei where these circles are shown in pink, no photo-CIDNP signal could be assigned, and hence, no experimental information on the ΔA_k is available.

Given the uncertainties in estimating T_{1T} (vide supra) and the remaining differences between experimental and simulated spectra, the hyperfine anisotropies ΔA_k listed in Table S1 should be considered as approximate. We wish to stress, however, that the distribution implied by the red circles in Figure 5 must be semiquantitatively correct, since spin dynamics is very sensitive to relative hyperfine couplings within the field range of more than 1 order of magnitude that we have studied here and agreement between experiment and simulation is good throughout this field range (Figure S6).

In a simple picture, the electron spin density of the ^{3}P state can be rationalized in terms of a linear combination of that of a single-electron occupied HOMO and of a single-electron occupied LUMO. Since the electron spin density in the radical cation state, which is related to the HOMO, has been demonstrated to be shifted to the L cofactor,[6,29,41] our data suggest that the LUMO is somewhat shifted to the M cofactor. That is indeed in line with the tentative interpretation of results from ^{1}H ENDOR spectroscopy on ^{3}P.[42] In Figure 5, the pink circles correspond to atoms that should have significant LUMO electron density and small HOMO electron density.

2. Longitudinal Relaxation Times of the Nuclei and of the Electron Spin in the Donor Triplet State. The empirical power law $T_{1T} = 22.2\cdot(17.6\ \mathrm{T}/B_0)^{0.69}$ ns, together with the Redfield-regime expression, eq 1, provides a good global fit of our data over more than 1 order of magnitude variation in the external magnetic field and qualitative agreement with the observed trends in signal intensity for R26 and WT RCs.

Nevertheless, the absolute values of T_{1T} provided by the power law and even the trend with magnetic field cannot be taken for granted, as the Redfield assumptions underlying eq 1 are violated. In any case, the longitudinal relaxation times of the electron spins in the donor triplet predicted by this equation at a nominal temperature of 235 K are within an order of magnitude of the one measured at 0.35 T by Hoff et al. along the *y* direction of the zero-field splitting tensor at 233 K.[34] This answers the long-standing question[32] whether the DR mechanism in the solid state, as originally suggested by Goldstein and Boxer,[25] is a consistent explanation for the enhanced absorptive signals observed in *R. sphaeroides* R26 photosynthetic RCs.

Uncertainties about the Redfield approximation do not affect our conclusion about a scaling of nuclear longitudinal relaxation times with magnetic field with a scaling exponent of about 1.31. This scaling is directly encoded in relative emissive and enhanced absorptive NMR line intensities for R26 RCs at fields between 4.7 and 17.6 T and a lower bound on nuclear relaxation time for WT RCs at 2.4 and 1.4 T. The lower bound depends on the assumption that nuclear relaxation times are the same in donor triplets of WT and R26 RCs, which cannot be taken for granted either, since the environment of the special pair differs due to presence or absence of a carotenoid. However, even if the lower bound is discarded, only the uncertainty of the scaling exponent increases. In that case, the scaling exponents between 1.1 and 1.6 are consistent with our data, whereas the lower limit implies two times faster nuclear relaxation at 17.6 T than was used for the simulations shown in Figure S6. If nuclear relaxation is the same in WT and R26 donor triplets, uncertainty of the scaling exponent reduces to the range between 1.1 and 1.4.

3. Field Dependence of the Solid-State Photo-CIDNP Mechanisms. For photosynthetic RCs of the carotenoidless R26 strain of *R. sphaeroides*, maximum polarization enhancement by the DR mechanism occurs at lower fields than maximum enhancement due to the TSM and DD mechanisms. The optimum field for DR enhancement is predicted to be even lower for WT RCs. This leads to a dominance of the DR mechanism at low fields, which improves the stringency of experimental tests of quantum-chemically computed triplet spin densities.

The optimum field for sensitivity enhancement depends on the information that one seeks in the NMR spectra. If chemical shift assignments and magnetic parameters in the paramagnetic states with atomic resolution are requested, signal-to-noise ratio has to be compared at the same chemical shift resolution. This is possible, since in any spectroscopy sensitivity can be traded for resolution by deconvolution-convolution techniques, as we have applied them to the spectrum shown in Figure 9. In this case, sensitivity for R26 RCs with dominating DR effect is optimum at fields between 4.7 and 9.4 T.

In other cases, it may be sufficient to detect and roughly assign polarization enhanced signals. Sensitivity is then proportional to $pB_0^{1/2}$, where p is the nuclear polarization. For R26 RCs, the optimum is then achieved at fields between 1.4 and 2.4 T.

Polarization enhancement with respect to thermal equilibrium polarization scales with p/B_0. This parameter increases with decreasing field for all nuclei within the whole field range that we have simulated ($B_0 > 0.25$ T). Note however that the field dependence of this enhancement is of practical relevance only if contrast between polarization enhanced and thermal equilibrium signals needs to be optimized.

4. Photo-CIDNP MAS NMR as Enhancement Method for Solid-State NMR. We have shown that the high-field TSM and DD mechanisms acting in RCs of *R. sphaeroides* show a maximum, which is around 2 T, as it is expected for a matching mechanism. The maximal effect might well be encountered at lower fields for other electron transfer systems as blue light photoreceptors and artificial reaction centers, which may have weaker ^{13}C hyperfine couplings or smaller *g* value differences. In fact, the only observation of the solid-state photo-CIDNP effect in a nonphotosynthetic system, a mutated blue-light photoreceptor,[15] was achieved at a rather low field of 2.4 T. Hence, application of lower fields might be a key to develop photo-CIDNP MAS NMR into a more generally applicable method for signal enhancement in solid-state NMR.

The main difficulty with such an approach is a loss of chemical shift resolution at lower fields, which is equivalent to a loss in effective sensitivity (vide supra). This problem could be circumvented by polarizing at lower fields than detecting, which requires shuttling of the sample between regions of the magnet with different field.[43,44] General application of solid-state photo-CIDNP would require artificial electron transfer systems which could be applied to surfaces and cavities in 'spin-torch' experiments in which the photo-CIDNP is transferred to explore the environment.

Our simulations indicate that much higher nuclear polarization can be obtained under optimized DR conditions than with the TSM and DD mechanisms (Figure 10). This is plausible, since the TSM and DD mechanisms depend on electron—nuclear spin state mixing near an avoided level crossing, which cannot be optimized for all nuclei at the same time and on a second matching condition, which cannot be controlled. This second matching is between the time scales of radical pair decay and hyperfine evolution for the DD mechanism or the electron Zeeman difference frequency and nuclear Zeeman frequency for the TSM mechanism.

In contrast, the DR mechanism depends on RPM polarization, which can lead to values of p of the order of unity. This polarization is completely retained in the ground state if nuclear spin longitudinal relaxation in the triplet state is much faster than triplet decay. Our simulations demonstrate that this situation can be attained for many nuclei in R26 RCs at fields lower than 2.4 T. Hence, it appears feasible to achieve high absolute polarization of several percent also for artificial systems.

■ MATERIALS AND METHODS

Sample Preparation. RCs from *R. sphaeroides* WT were isolated as described by Shochat et al.;[45] RCs from *R. sphaeroides* R26 were isolated by the procedure of Feher and Okamura.[46] The removal of Q_A has been done by incubating the RCs at a concentration of 0.6 μM in 4% LDAO, 10 mM *o*-phenanthroline, 10 mM Tris buffer, pH 8.0, for 6 h at 26 °C, followed by washing with 0.5 M NaCl in 10 mM Tris buffer, pH 8.0, containing 0.025% LDAO and 1 mM EDTA.[47] Approximately 5 mg of the RC protein complex embedded in LDAO micelles was used for NMR measurements.

MAS NMR Measurements. The NMR experiments at different fields were performed with DSX-750, DMX-400, DMX-200, AV-100 and AV-60 NMR spectrometers equipped with MAS probe (Bruker, Karlsruhe, Germany). The sample was loaded into a clear 4-mm sapphire rotor and inserted into the MAS probe. The sample was frozen slowly at a low spinning frequency of ν_r = 400 Hz to ensure a homogeneous sample distribution against the rotor wall.[48] The light and dark spectra were collected with a Hahn echo pulse sequence and TPPM proton decoupling.[49] The hardware of the spectrometer does not allow for proton decoupling below the magnetic field of 2.4 T. Therefore, spectra below the magnetic field of 2.4 T were measured by an antiringing pulse sequence.[50] All ^{13}C MAS NMR spectra were obtained at a temperature of 235 K under the continuous illumination of white light.[51]

The rotational frequency for MAS was 8 kHz in all experiments. For the five fields of 1.4, 2.4, 4.7, 9.4, and 17.6 T, a line broadening of 10, 10, 20, 50, and 120 Hz, respectively, was applied prior to the Fourier transformation. In all cases, a cycle delay of 4 s was used. All the ^{13}C MAS NMR spectra were referenced to TMS by using the $^{13}COOH$ response of solid tyrosine·HCl at 172.1 ppm.

Simulations. Hyperfine anisotropies in the donor triplet state were computed with ADF 2004.1,[52,53] employing the BLYP functional[36,37] and DP basis sets for all nuclei based on the special pair structure from *R. sphaeroides* R26 in the charge-neutral state (PDB entry 1AIJ)[35] and with ADF 2009.1[52,54] utilizing a TZP basis set and the BP86 functional.[36,39] The coordinates from the charge-neutral state of *R. sphaeroides* WT (PDB entry 1PCR)[55] have been amended with hydrogen atoms and optimized in TURBOMOLE V6.0. For the geometry optimization, a TZVP[56] basis and the BP86 functional have been used in combination with the RI approximation using the standard TZVP basis set from TURBOMOLE.[57,58] Coordinates were first optimized for the radical cation state and these finally relaxed in the ^3P configuration (for coordinates and absolute energies see Supporting Information). DR intensities have been simulated by a home-written Matlab program as described in ref 7 assuming that the nuclear longitudinal relaxation rate constant $1/T_1$ is proportional to the square of hyperfine anisotropy ΔA^2. Here, ΔA is defined as $3(A_z - a_{\mathrm{iso}})/2$, where A_z is the largest eigenvalue of the hyperfine tensor and a_{iso} is its trace. Since $\Delta A = 3\gamma_I^2\gamma_S^2\hbar^2\mu_0^2/(16\pi^2 r^6)$ for the point-dipole approximation used by Abragam,[33] a factor 9 is introduced in the numerator of eq 1. Further details have been given above. The program is available from the authors upon request.

Abbreviations. BChl, bacteriochlorophyll; BPhe, bacteriopheophytin; DD, differential decay; DFT, density functional theory; DR, differential relaxation; EDTA, ethylene diamino tetra acetate; hfc, hyperfine coupling; HOMO, highest occupied molecular orbital; LDAO, *N*,*N*-dimethyl dodecylamine-*N*-oxide; LOV, light oxygen voltage; LUMO, lowest unoccupied molecular orbital; MAS, magic angle spinning; NMR, nuclear magnetic resonance; P, special pair primary electron donor; photo-CIDNP, photochemically induced dynamic nuclear polarization; Q_A, ubiquinone; *R.*, *Rhodobacter*; RC, reaction center; RPM, radical pair mechanism; S, singlet; T_0, triplet; TPPM, two pulse-phase modulation; TSM, electron electron nuclear three spin mixing; WT, wild type.

■ ASSOCIATED CONTENT

Ⓢ Supporting Information

^{13}C photo-CIDNP MAS NMR spectra with and without ^1H decoupling, fit for obtaining scaling factors for simulated peak intensities, spin density distribution in the geometry optimized triplet state, simulations based on optimized coordinates and crystallographic coordinates, field dependent spectral simulations and intensity calculations, calculated ^{13}C hyperfine anisotropies, and absolute energies and Cartesian coordinates for optimized structures. This material is available free of charge via the Internet at http://pubs.acs.org.

■ AUTHOR INFORMATION

Corresponding Author

gunnar.jeschke@phys.chem.ethz.ch; j.matysik@chem.leidenuniv.nl

Notes

The authors declare no competing financial interest.

■ ACKNOWLEDGMENTS

The authors thank Dr. B. Anger for exciting discussions, Prof. J. Neugebauer for the kind gift of computation time and Prof. H. de Groot for continuous interest. Support from F. Lefeber, and K. Erkelens during various stages of the experiments is gratefully acknowledged. The authors thank NWO for generous support (ALW open competitie, 818.02.019; Middelgroot 700.57.107). This work has been supported by a Feodor-Lynen fellowship by the Alexander von Humboldt Foundation financed by the German Federal Ministry of Education and Research and a Marie Curie Intra European Fellowship within the 7th European Community Framework Programme.

■ REFERENCES

(1) Maier, G.; Haeberlen, U.; Wolf, H. C.; Hausser, K. H. *Phys. Lett.* **1967**, *25A*, 384−385.

(2) Stehlik, D.; Colpa, J. P. *Chem. Phys.* **1977**, *21*, 273−288.

(3) Zysmilich, M. G.; McDermott, A. *J. Am. Chem. Soc.* **1994**, *116*, 8362−8363.

(4) Jeschke, G.; Matysik, J. *Chem. Phys.* **2003**, *294*, 239−255.

(5) Daviso, E.; Jeschke, G.; Matysik, J. In *Biophysical Techniques in Photosynthesis II*; Aartsma, T. J., Matysik, J., Eds.; Springer: Dordrecht; 2008, pp 385−399.

(6) Prakash, S.; Alia; Gast, P.; de Groot, H. J. M.; Jeschke, G.; Matysik, J. *J. Am. Chem. Soc.* **2005**, *127*, 14290−14298.

(7) Prakash, S.; Alia; Gast, P.; de Groot, H. J. M.; Matysik, J.; Jeschke, G. *J. Am. Chem. Soc.* **2006**, *128*, 12794−12799.

(8) Janssen, G. J.; Daviso, E.; van Son, M.; de Groot, H. J. M.; Alia, A.; Matysik, J. *Photosynth. Res.* **2010**, *104*, 275−282.

(9) Matysik, J.; Alia; Gast, P.; van Gorkom, H. J.; Hoff, A. J.; de Groot., H. J. M. *Proc. Natl. Acad. Sci. U.S.A.* **2000**, *97*, 9865−9870.

(10) Alia; Roy, E.; Gast, P.; van Gorkom, H. J.; de Groot, H. J. M.; Jeschke, G.; Matysik, J. *J. Am. Chem. Soc.* **2004**, *126*, 12819−12826.

(11) Diller, A.; Roy, E.; Gast, P.; van Gorkom, H. J.; de Groot, H. J. M.; Glaubitz, C.; Jeschke, G.; Matysik, J.; Alia, A. *Proc. Natl. Acad. Sci. U.S.A.* **2007**, *104*, 12767−12771.

(12) Roy, E.; Alia; Gast, P.; van Gorkom, H. J.; de Groot, H. J. M.; Jeschke, G.; Matysik, J. *Biochem. Biophys. Acta* **2007**, *1767*, 610−615.

(13) Roy, E.; Rohmer, T.; Gast, P.; Jeschke, G.; Alia, A.; Matysik, J. *Biochemistry* **2008**, *47*, 4629−4635.

(14) Matysik, J.; Diller, A.; Roy, E.; Alia, A. *Photosynth. Res.* **2009**, *102*, 427−435.

(15) Thamarath, S. S.; Heberle, J.; Hore, P. J.; Kottke, T.; Matysik, J. *J. Am. Chem. Soc.* **2010**, *132*, 15542−15543.

(16) Daviso, E.; Alia, A.; Prakash, S.; Diller, A.; Gast, P.; Lugtenburg, J.; Jeschke, G.; Matysik, J. *J. Phys. Chem. C* **2009**, *113*, 10269−10278.

(17) Hoff, A. J.; Deisenhofer, J. *Phys. Rep.* **1997**, *287*, 2−247.

(18) Hunter, C. N.; Daldal, F.; Thurnauer, M. C.; Beatty, J. T. The Phototropic Purple Bacteria. In *Advances in Photosyntheis and Respiration*; (Series Editor Govindjee); Springer: Dordrecht, 2008; Vol. *28*.

(19) Jeschke, G. *J. Chem. Phys.* **1997**, *106*, 10072−10086.

(20) Jeschke, G. *J. Am. Chem. Soc.* **1998**, *120*, 4425−4429.

(21) Polenova, T.; McDermott, A. E. *J. Phys. Chem. B.* **1999**, *103*, 535−548.

(22) Closs, G. L.; Closs, L. E. *J. Am. Chem. Soc.* **1969**, *91*, 4549−4550.

(23) Kaptein, R.; Oosterhoff, J. L. *Chem. Phys. Lett.* **1969**, *4*, 195−197.

(24) Closs, G. L. *Chem. Phys. Lett.* **1975**, *32*, 277−278.

(25) Goldstein, R. A.; Boxer, S. G. *Biophys. J.* **1987**, *51*, 937−946.

(26) Hore, P. J.; Broadhurst, R. W. *Prog. Nucl. Magn. Reson. Spectrosc.* **1993**, *25*, 345−402.

(27) Marchanka, A.; Paddock, M.; Lubitz, W.; van Gastel, M. *Biochemistry* **2007**, *46*, 14782−14794.

(28) Marchanka, A.; Savitsky, A.; Lubitz, W.; Möbius, K.; van Gastel, M. *J. Phys. Chem. B* **2010**, *114*, 14364−14372.

(29) Daviso, E.; Prakash, S.; Alia, A.; Gast, P.; Neugebauer, J.; Jeschke, G.; Matysik, J. *Proc. Natl. Acad. Sci. U.S.A.* **2009**, *106*, 22281−22286.
(30) Diller, A.; Prakash, S.; Alia, A.; Gast, P.; Matysik, J.; Jeschke, G. *J. Phys. Chem. B.* **2007**, *111*, 10606−10614.
(31) Jeschke, G.; Anger, B. C.; Bode, B. E.; Matysik, J. *J. Phys. Chem. A.* **2011**, *115*, 9919−9928.
(32) McDermott, A.; Zysmilich, M. G.; Polenova, T. *Solid State Nucl. Magn. Reson.* **1998**, *11*, 21−47.
(33) Abragam, A. *Principles of Nuclear Magnetism*; Oxford University Press: Oxford, U.K., 1962.
(34) Hoff, A. J.; Proskuryakov, I. I. *Chem. Phys. Lett.* **1985**, *115*, 303−310.
(35) Stowell, M. H.; McPhillips, T. M.; Rees, D. C.; Soltis, S. M.; Abresch, E.; Feher, G. *Science* **1997**, *276*, 812−816.
(36) Becke, A. D. *Phys. Rev. A* **1988**, *38*, 3098.
(37) Lee, C.; Yang, W.; Parr, R. G. *Phys. Rev. B* **1988**, *37*, 785.
(38) Ahlrichs, R.; Bär, M.; Häser, M.; Horn, H.; Kälmel, C. *Chem. Phys. Lett.* **1989**, *162*, 165.
(39) Perdew, J. P.; Wang, Y. *Phys. Rev. B* **1986**, *33*, 8822.
(40) Kaptein, R. *J. Chem. Soc., Chem. Commun.* **1971**, 732−733.
(41) Lendzian, F.; Huber, M.; Isaacson, R. A.; Endeward, B.; Plato, M.; Bönigk, B.; Möbius, K.; Lubitz, W.; Feher, G. *Biochim. Biophys. Acta* **1993**, *1183*, 139−160.
(42) Lubitz, W.; Lendzian, F.; Bittl, R. *Acc. Chem. Res.* **2002**, *35*, 313−320.
(43) Grosse, S.; Gubaydullin, F.; Scheelken, H.; Vieth, H. M.; Yurkovskaya, A. V. *Appl. Magn. Reson.* **1999**, *17*, 211−225.
(44) Ivanov, K. L.; Miesel, K.; Yurkovskaya, A. V.; Korchak, S. E.; Kiryutin, A. S.; Vieth, H. M. *Appl. Magn. Reson.* **2006**, *30*, 513−534.
(45) Shochat, S.; Arlt, T.; Francke, C.; Gast, P.; Vannoort, P. I.; Otte, S. C. M.; Schelvis, H. P. M; Schmidt, S.; Vijgenboom, E.; Vrieze, J.; Zinth, W.; Hoff, A. J. *Photosynth. Res.* **1994**, *40*, 55−66.
(46) Feher, D.; Okamura, M. Y. In *The Photosynthetic Bacteria*; Clayton, R. K., Siström, W., Eds.; Plenum Press: New York, 1978; p 349−378.
(47) Okamura, M. Y.; Isaacson, R. A.; Feher, G. *Proc. Natl. Acad. Sci. U.S.A.* **1975**, *72*, 3491−3495.
(48) Fischer, M. R.; de Groot, H. J. M.; Raap, J.; Winkel, C.; Hoff, A. J.; Lugtenburg, J. *Biochemistry* **1992**, *31*, 11038−11049.
(49) Bennett, A. E.; Rienstra, C. M.; Auger, M.; Lakshmi, K. V.; Griffin, R. G. *J. Chem. Phys.* **1995**, *103*, 6951−6958.
(50) Zhang, S.; Wu, X.; Mehring, M. *Chem. Phys. Lett.* **1990**, *173*, 481−484.
(51) Matysik, J.; Alia; Hollander, J. G.; Egorova-Zachernyuk, T.; Gast, P.; de Groot, H. J. M. *Indian J. Biochem. Biophys.* **2000**, *37*, 418−423.
(52) te Velde, G.; Bickelhaupt, F. M.; van Gisbergen, S. J. A.; Fonseca Guerra, C.; Baerends, E. J.; Snijders, J. G.; Ziegler, T. J. *Comput. Chem.* **2001**, *22*, 931.
(53) *ADF2004.01*, SCM, Theoretical Chemistry, Vrije Universiteit: Amsterdam, The Netherlands; http://www.scm.com.
(54) *ADF2009.01*, SCM, Theoretical Chemistry, Vrije Universiteit: Amsterdam, The Netherlands; http://www.scm.com.
(55) Dunning, T. H. Jr. *J. Chem. Phys.* **1989**, *90*, 1007.
(56) Ermler, U.; Fritzsch, G.; Buchanan, S. K.; Michel, H. *Structure* **1994**, *2*, 925−936.
(57) Eichkorn, K.; Treutler, O.; Öhm, H.; Haser, M.; Ahlrichs, R. *Chem. Phys. Lett.* **1995**, *242*, 652.
(58) Eichkorn, K.; Weigend, F.; Treutler, O.; Ahlrichs, R. *Theor. Chem. Acc.* **1997**, *97*, 119.